Electronic Supplementary Material (ESI) for Sustainable Energy & Fuels.

Supporting Information

Crystal Size-Controlled Growth of Bismuth Vanadate for Highly Efficient Solar Water Oxidation

Qi Qin [a], Qian Cai [a], Chuangyong Jian [a,b], and Wei Liu *[a]

[a.] CAS Key Laboratory of Design and Assembly of Functional Nanostructures, Fujian Provincial Key Laboratory of Nanomaterial, Fujian Institute of Research on the Structure of Matter, Chinese Academy of Sciences, Fuzhou, Fujian, 350002, China

[b.] University of Chinese Academy of Sciences, Beijing, 100049, China

1. Experimental section

1.1. Materials synthesis

1.1.1. Fabrication of BVO films

Firstly, 4.366g of $Bi(NO_3)_3 \cdot 5H_2O$ and 1.351g of 2, 3-Dihydroxybernsteinsaeure were dissolved into 30ml of DI water to prepare Bi precursor solution. Subsequently adding 1 M NaOH solution slowly into the above solution, and the pH of the solution was adjusted to 9, 11 and 13 respectively. A typical three-electrode cell was used for electrodeposition in this alkaline electrolyte. The external bias was maintained at 2.3 V vs. RHE with deposition times (2 min). Finally, the obtained Bi_2O_3 films were filtered, washed, and dried. To convert the Bi precursor films to BVO photoanode films, 30 mg $VO(acac)_2$ was placed evenly on a crucible plate and then putting the FTO glass substrate above. The films electrode was heated in a muffle furnace at 500°C for 2 h in the air to convert bismuth precursor films to BVO photoanode. The films were soaked in 1 M NaOH solution for 15 min with gentle stirring to remove the excess surface V_2O_5 of BVO photoanode films. The BVO samples are named according to their pH of precursor as follows: BVO-1 (pH=9), BVO-2 (pH=11) and BVO-3(pH=13).

1.1.2. Fabrication of Fe-Pi OECs

Fe-Pi was fabricated on the basis of the method reported in a recent study with a few modifications. In brief, the BVO substrate obtained was immersed in 30 mM $FeCl_3$ aqueous solution for 20 s to absorb iron cations onto the substrate due to electrostatic attraction between the metal ions and the substrate. Then, the substrate was immersed in 15 mM Na_2HPO_4 aqueous solution for another 20 s. The cycle was repeated 5 times to obtain an optimum loading amount. Finally, the coated films rinsed with deionized water and dried in the air

1.2. Materials characterization

Crystal structure of electrodes was examined by Film-XRD (D8 Advance, Bruker) with Cu K_α (λ =0.15406 nm) radiation) and Raman spectrum of the films were obtained on a Labram HR Evolution (Horiba Jobin Yvon). The crystal morphologies of the electrodes were examined with Field-emission Scanning Electron Microscopy (FESEM) (HITACHI UHR FE-SEM SU8010). Transmission electron microscopy (TEM), high-resolution transmission electron microscopy (HRTEM), and imaging were performed with an FEI Tecnai F20 microscope with an

accelerating voltage of 200 kV. XPS measurements are conducted using an ESCALAB 250Xi system (Thermo Fisher) to investigate the chemical states and composition of the films, which is equipped with a 100 W Al Kα source on a spot size of 100 μm at 45° incident angle. The binding energy scale is calibrated to carbon line of 284.8 eV. UV-vis absorption spectra of the films were obtained on a Lambda950 spectrophotometer (PerkinElmer). A Varian GC-3380 gas chromatograph was used to determine the amount of oxygen and hydrogen produced with nitrogen as the carrier gas.

2. Photoelectrochemical measurements

Photoelectrochemical performances of photoanodes are performed on a CHI660e electrochemical workstation with a standard three-electrode cell at room temperature. PEC performance of the obtained $BiVO_4$ films as the working electrode without further treatments was measured using a typical three-electrode cell. Pt wire is used as the counter electrode and Ag/AgCl electrode filled with 3.5 M KCl serves as the reference electrode. A Xenon 150 W lamp was employed as the light source. Light was illuminated through an AM 1.5 G filter and the power density of the incident light was calibrated to 100 mW/cm^2 at the surface of the FTO substrate by using a thermopile detector. For water oxidation, the electrolyte of all electrochemical measurements was a 1 M potassium borate solution, while as a hole scavenger 0.2 M Na_2SO_3 (98%, Sigma-Aldrich) was added to above electrolyte and significantly improved the charge separation efficiencies. Photocurrent-potential curves were monitored using linear sweep voltammogram in a voltage window of 0.2~1.3 V vs. RHE with a scan rate of 50 mV/s. The conversion between potentials vs. Ag/AgCl and vs. RHE is performed according to the Nernst equation below: [1]

$$E_{RHE} = E_{Ag/AgCl} + 0.059 * pH + E^0_{Ag/AgCl}$$

Where E_{RHE} is the potential referred to a reversible hydrogen electrode (RHE), and $E_{Ag/AgCl}$ is the measured potential against Ag/AgCl reference electrode.

Applied bias photon-to-current efficiency (ABPE) can be calculated using the following equation:[2]

$$\text{ABPE}\ (\%) = \frac{(1.23 - V_b) \times J_{ph}}{P_{light}} \times 100\%$$

Where J_{ph} presents the photocurrent density ($mW \cdot cm^{-2}$) obtained from the electrochemical workstation. V_b refers to the applied bias vs. RHE (V), and P_{total} is the total light intensity of AM 1.5 G (100 $mV \cdot cm^{-2}$).

The incident-photon-to-current-efficiency (IPCE) as a function of wavelength for the prepared photoanodes was measured at a bias of 1.23 V vs. RHE by a CHI660e electrochemical workstation, and the monochromator was incremented in the spectral range (300-600 nm) with a sampling interval of 20 nm and a current sampling time of 10 s. The IPCE was calculated by equation: [2]

$$\text{IPCE}\ (\%) = \frac{1240 \times J_{ph}}{P_{mono} \times \lambda} \times 100\%$$

Where J_{ph} presents the photocurrent density ($mW \cdot cm^{-2}$) obtained from the electrochemical workstation. P_{mono} is the intensity of the incident monochromatic light ($mW \cdot cm^{-2}$), and λ is the wavelength (nm) of the monochromatic light.

Applied bias photon-to-current efficiency (ABPE) can be calculated using the following equation:[2]

$$\text{ABPE}\ (\%) = \frac{(1.23 - V_b) \times J_{ph}}{P_{light}} \times 100\%$$

Where J_{ph} presents the photocurrent density ($mW \cdot cm^{-2}$) obtained from the electrochemical workstation. V_b refers to the applied bias vs. RHE (V), and P_{total} is the total light intensity of AM 1.5 G (100 $mV \cdot cm^{-2}$).

To confirm the inference, we calculated the transient decay time using the following equation: [3]

$$D = \frac{I_t - I_s}{I_m - I_s}$$

Where I_t represents current at time t, Is represents the stabilized current, and I_m represents the current spike. The transient decay time can be defined as the time at which Ln D = -1.

Electrochemical impedance spectroscopy (EIS) measurements for all the photoanodes was conducted by applying AC voltage amplitude of 10 mV within the frequency range from 10^5 to 10^{-2} Hz.

Photocurrent density obtained for sulfite oxidation was used to calculate $\eta_{abs} \times \eta_{sep}$ by using Eq.1, where J_{PEC} is the practical photocurrent density of the BVO photoanodes, J_{max} is the theoretical photocurrent density (7.5 mA cm^{-2}), η_{abs} is the light absorption efficiency, $\eta_{transport}$ is the charge transport efficiency, and $\eta_{transfer}$ is the charge transfer efficiency at the interface between the surface and electrolyte. [3]

$$J_{PEC} = J_{max} \times \eta_{abs} \times \eta_{transport} \times \eta_{transfer} \quad (1)$$

For sulfite oxidation with extremely fast oxidation kinetics, the surface charge transfer efficiency of the photoanode ($\eta_{transfer}$) is ≈ 1. Therefore, we can define the $\eta_{abs} \times \eta_{stransport} \approx J_{sulfite} / J_{max}$, where $J_{sulfite}$ is the photocurrent density for sulfite oxidation.

Mott-Schottky (MS) spectra were measured in the dark (increment: 10 mV, open circles: 1000 Hz, filled circles: 500 Hz).

Faradaic efficiency of water splitting was calculated by dividing the amount of the experimentally generated gas by the theoretical amount of gas which is calculated by the charge passed through the electrode: [4]

Faradaic $efficiency_{O2} = = V_{experiment} / V_{theoretical} = V_{experiment} / [(1/4)*(Q/F)*V_m]$

where Q is the summation of the charge passed through the electrodes, F is the Faraday constant (96485 C mol^{-2}), V_m is the molar volume of gas (24.1 L mol^{-1} , 293 K, , 101 kPa).

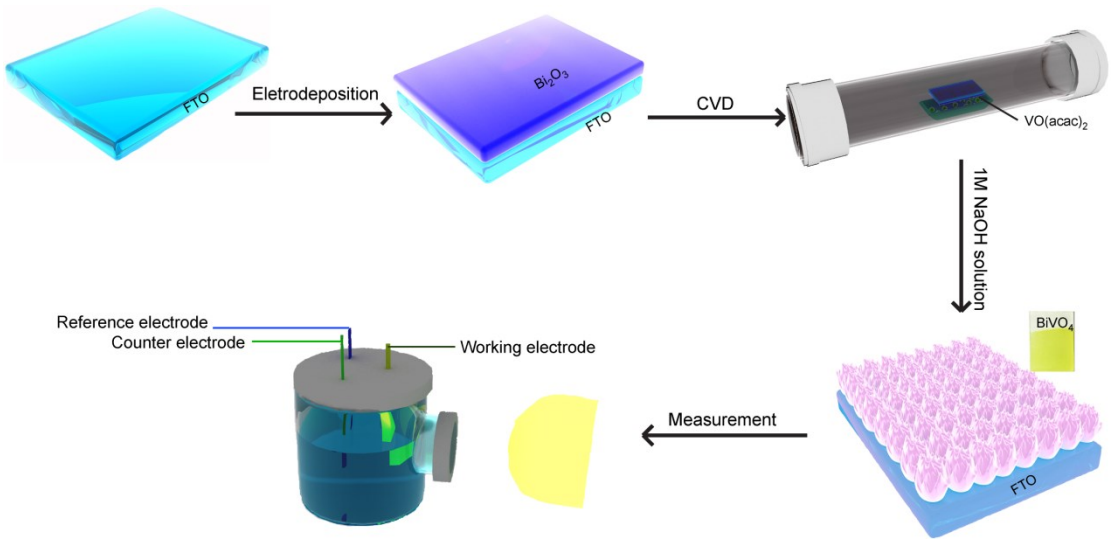

Figure S1. (a) Schematic of the fabrication process flow of $BiVO_4$ films.

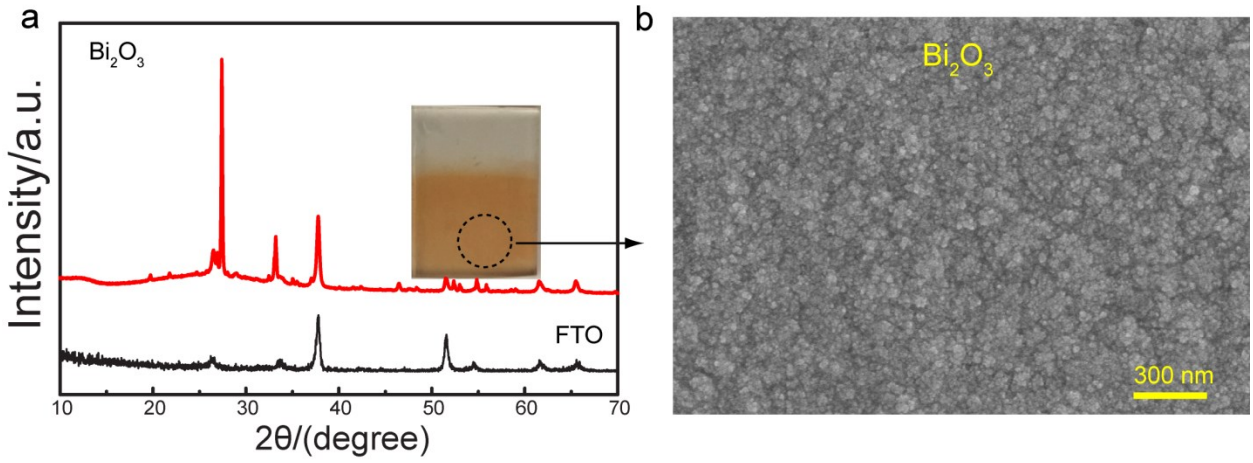

Figure S2. a) and b) X-ray diffraction pattern and SEM images of Bi_2O_3 film on FTO.

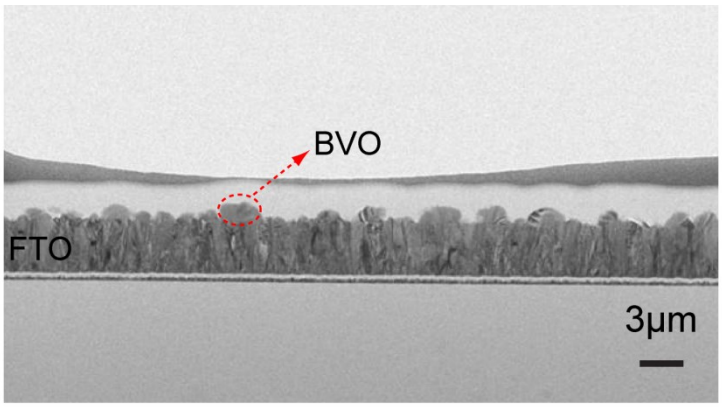

Figure S3. TEM image of the FTO/BVO-3 films.

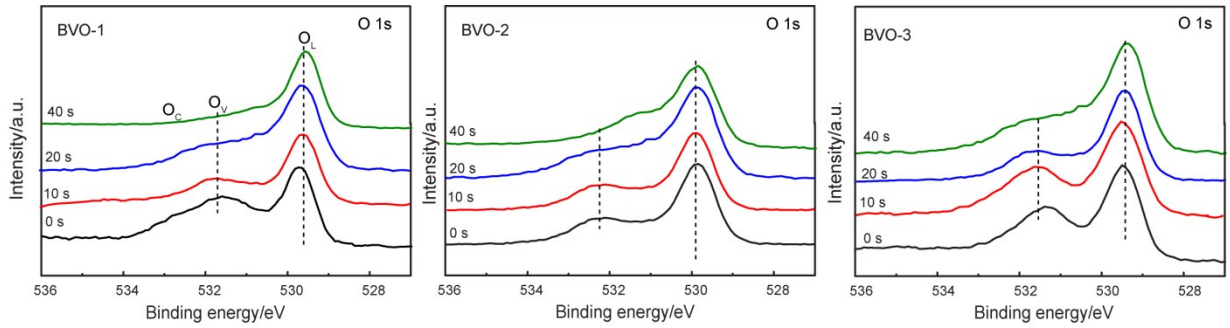

Figure S4. Depth-profile XPS of different BVO.

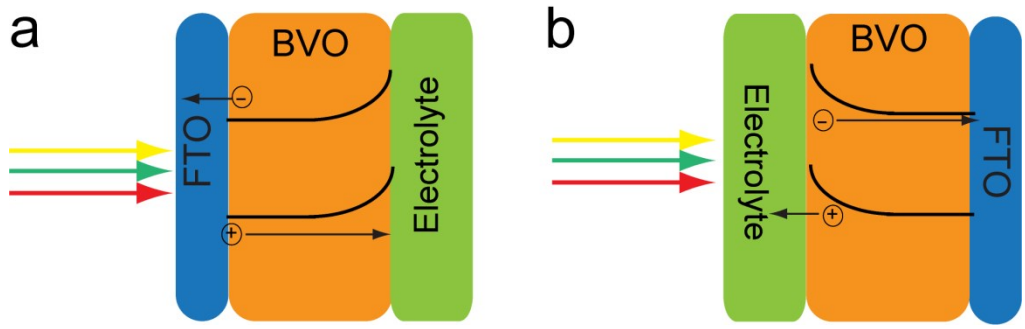

Figure S5. Schematic of exhibiting different photocurrent densities under front and back side illumination. Backside lighting generates electron-hole pairs near the FTO conductive substrate, while front-side lighting generates electron-hole pairs near the BVO photoanode film/electrolyte interface. Since electrons need to reach the FTO substrate and holes need to reach the electrolyte, slower electron transport and longer distances will result in excessive electron-hole recombination. Therefore, the BVO photoanode film can achieve the best photocurrent density under backlighting.

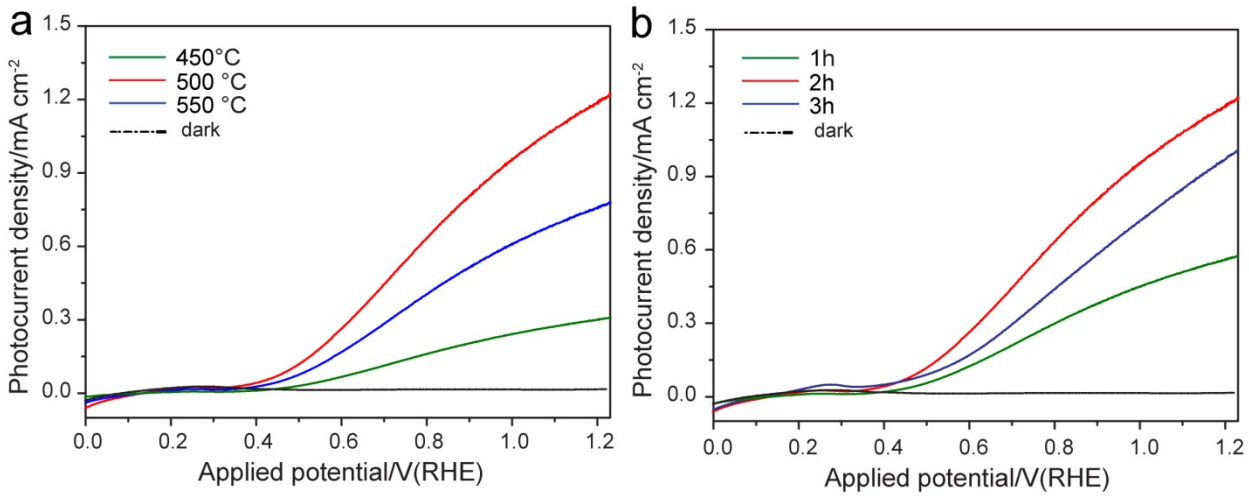

Figure S6. Photocurrent density vs. applied potential curves of the BVO-3 films of a) different calcination temperature and b) different annealing duration time at 500 °C in air under back illumination through an AM 1.5 G filter with the intensity of 100 mW • cm^{-2} in 1 M potassium electrolyte.

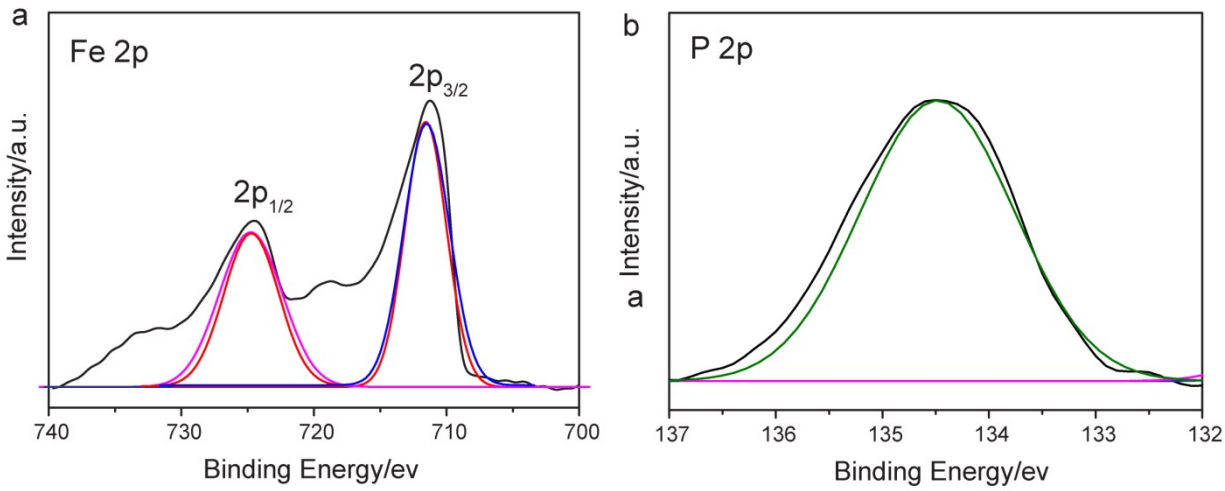

Figure S7. XPS spectra of (a) Fe 2p, (b) P 2p for the FTO/BVO-3/Fe-Pi films.

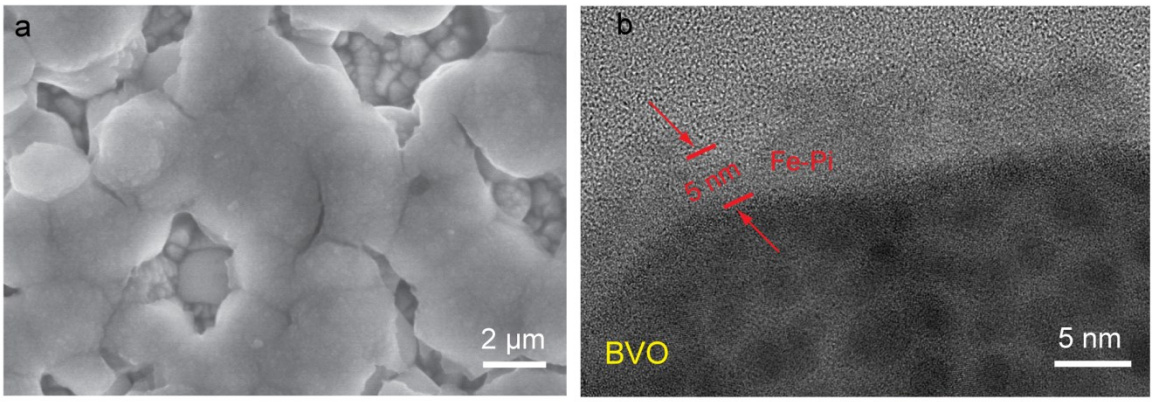

Figure S8. (a) Top-view SEM image and (b) TEM of FTO/BVO-a3/Fe-Pi films.

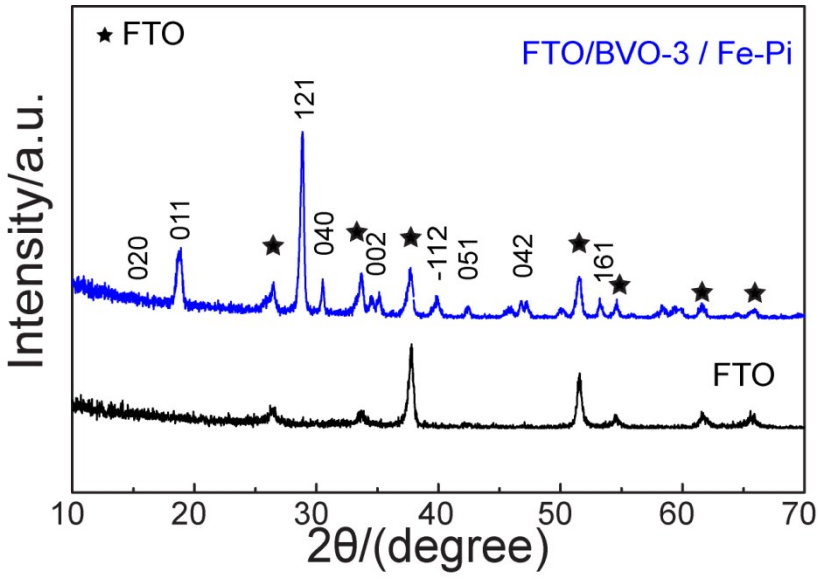

Figure S9. XRD pattern of FTO/BVO-3/Fe-Pi films.

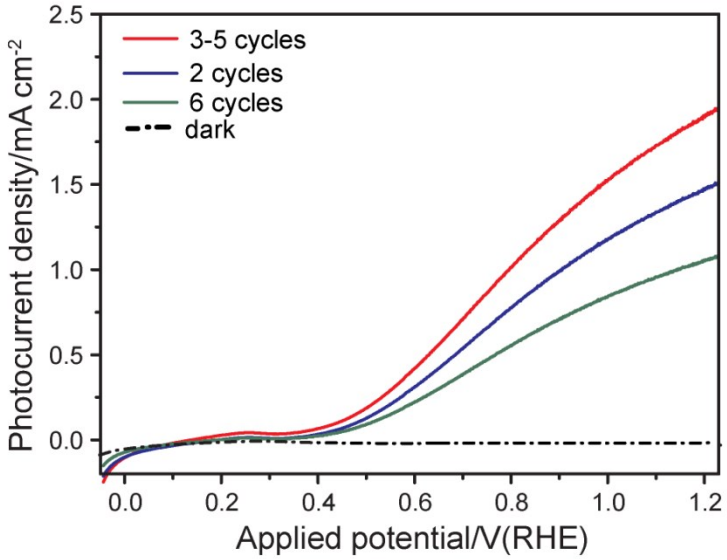

Figure S10. Photocurrent density vs. applied potential curves of the FTO/BVO-3/Fe-Pi films of different Fe-Pi deposition cycles under back illumination through an AM 1.5 G filter with the intensity of 100 mW • cm^{-2} in 1 M potassium electrolyte.

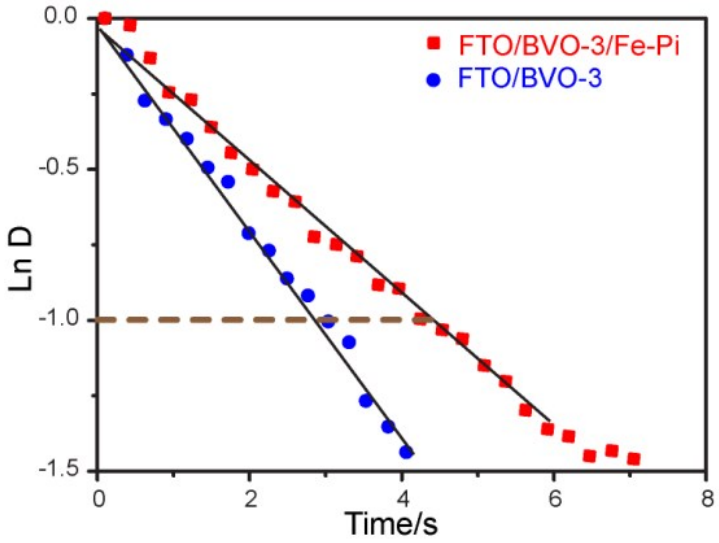

Figure S11. The decay of the bulk electrolysis current density over time under these conditions. The light turns on at 0s and turns off at 10s

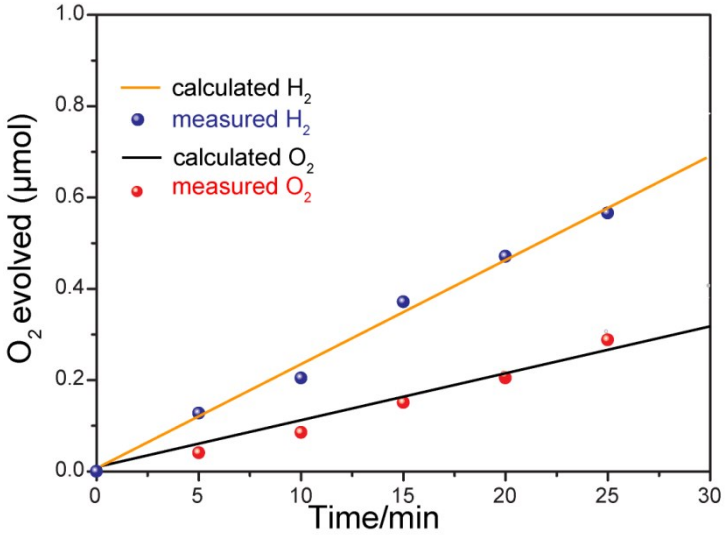

Figure S12. Fluorescence probe measurement of O_2 generation from a FTO/BVO-3/Fe-Pi electrode at 1.23 V vs RHE under AM 1.5G, 100 mW/cm^2 illumination.

Table S1. PEC performance comparison of $BiVO_4$ anodes reported in literature.

Catalyst	Crystallites diameter	pH	Cocatalyst	J[a] ($mA \cdot cm^{-2}$)	Reference
$BiVO_4$	~3.6 μ m	9.6	Fe-Pi	1.75	This work
$BiVO_4$	~1 μ m	9.6	CoOx	2.5	Adv. Energy Mater. 2018, 1802198.
$BiVO_4$	~100 nm	9.5	MDH	0.75	Energy Lett. 2017, 2, 1062.
$BiVO_4$	~100 nm	9.5	CoBi	2.5	Angew. 201703491.
$BiVO_4$	~200 nm	9	Fh	~1..5	ACS Catal.2017, 7, 1868.
$BiVO_4$	~300 nm	9.5	/	~1	Angew. 2016, 55, 1769.
Co_3O_4/ $BiVO_4$	~150 nm	9.5	Co_3O_4	~0.6	J. Am. Chem. Soc. 2015, 137, 8356.
$BiVO_4$	~200 nm	9.4	Fe-Pi	2.28	Appl. Catal. B Environ. 2018.11.001
W: $BiVO_4$	~100 nm	9.5	Co-Pi	1	J. Am. Chem. Soc. 2011, 133, 18370.
$BiVO_4$	~300 nm	7	STO	0.8	Adv. Funct. Mater. 2019, 1902101.
$BiVO_4$	~100 nm	7	Bi_2O_3	2.2	ACS Appl. Mater. Interfaces. 2019, 11, 47, 44069

[a] refers the current density produced at 1.23 V vs RHE without sacrificial reagent

[1] L. Zhang, E. Reisner, J. J. Baumberg, *Energy Environ. Sci.* **2014**, *7*, 1402.

[2] Z. Chen, T. F. Jaramillo, T. G. Deutsch, A. Kleiman-Shwarsctein, A. J. Forman, N. Gaillard, R. Garland, K. Takanabe, C. Heske, M. Sunkara, E. W. McFarland, K. Domen, E. L. Miller, J. A. Turner, H. N. Dinh, *J Mater Res* **2010**, *25*, 3.

[3] L. Zhou, C. Zhao, B. Giri, P. Allen, X. Xu, H. Joshi, Y. Fan, L. V. Titova, P. M. Rao, *Nano Lett.* **2016**, *16*, 3463.

[4] Y. Li, J. Chen, P. Cai, Z. Wen, *J. Mater. Chem. A* **2018**, *6*.